

Effect of the Barometric Phase Transition of a DMPA Bilayer on the Lipid/Water Interface. An Atomistic Description by Molecular Dynamics Simulation

J. J. Giner Casares,[†] L. Camacho,[†] M. T. Martín Romero,[†] and J. J. López Cascales^{*‡}

Departamento Química Física y Termodinámica Aplicada, Ed. Marie Curie, Campus de Rabanales, Universidad de Córdoba, 14014 Córdoba, Spain, and Universidad Politécnica de Cartagena, Centro de Electroquímica y Materiales Inteligentes (CEMI), Aulario II, Campus de Alfonso XIII, 30203 Cartagena, Murcia, Spain

Received: July 27, 2007; In Final Form: September 24, 2007

Understanding the structure and dynamics of phospholipid bilayers is of fundamental relevance in biophysics, biochemistry, and chemical physics. Lipid Langmuir monolayers are used as a model of lipid bilayers, because they are much more easily studied experimentally, although some authors question the validity of this model. With the aim of throwing light on this debate, we used molecular dynamics simulations to obtain an atomistic description of a membrane of dimyristoylphosphatidic acid under different surface pressures. Our results show that at low surface pressure the interdigitation between opposite lipids (that is, back-to-back interactions) controls the system structure. In this setting and due to the absence of this effect in the Langmuir monolayers, the behavior between these two systems differs considerably. However, when the surface pressure increases the lipid interdigitation diminishes and so monolayer and bilayer behavior converges. In this work, four computer simulations were carried out, subjecting the phospholipids to lateral pressures ranging from 0.17 to 40 mN/m. The phospholipids were studied in their charged state because this approach is closer to the experimental situation. Special attention was paid to validating our simulation results by comparison with available experimental data, there being in general excellent agreement between experimental and simulation data. In addition, the properties of the lipid/solution interface associated with the lipid barometric phase transition were studied.

1. Introduction

This work was focused on the venerable and still prominent topic of lipid bilayer structure, which plays a crucial role controlling the diffusion of nutrients, ions, and water between the inner and outer cell together, while providing a suitable environment to other molecules embedded in the membrane, such as membrane proteins or cholesterol, among others.^{1,2} Understanding the atomic interactions that control the behavior of this complicated system is of unquestionable importance. One of the aspects that has attracted increasing interest during recent decades is the polymorphic phase transition of lipid bilayers associated with temperature due to the importance of this process from a biological viewpoint. In this respect, a temperature denoted transition temperature (T_m) defines the temperature at which lipids change from a gel (P_β) to a liquid crystalline state (L_α) at a constant external pressure.^{3,4}

However, polymorphic phase transition may also be associated with different states induced by an external pressures or barometric transition.^{5,6} To understand the atomic interactions that govern these phase transitions induced by an external pressure, Langmuir air–water lipid monolayers have been widely studied,⁷ mainly because they enable the surface pressure on the lipids that form the monolayer to be studied, and also because a monolayer is basically half of a symmetric lipid bilayer. For this purpose, different experimental techniques have

been used, such as scattering techniques, X-ray and neutron reflectivity measurements, infrared reflection–absorption spectrometry (IR), NMR studies, and the ellipsometric technique.^{7–13} In the case of monolayers, different barometric phases have been denoted, such as G (gaseous), LE (liquid expanded), LC (liquid condensed), and SC (solid condensed).⁷

Improvements made in simulation algorithm and the increases in the computing power attained during recent years have led to molecular dynamics simulation¹⁴ emerging as a powerful and precise technique that provides atomic insight into the dynamic and steady properties related with lipid bilayers and monolayers.^{15–19} Keeping this in mind with the aim of obtaining an atomic insight into the interactions that control the phase transition of a lipid bilayer, a computer simulation of a lipid bilayer of dimyristoylphosphatidic acid (DMPA[−]) was carried out. The main reasons why we chose this type of lipid instead of DPPC or DPPE were the following: first, because charged lipids at physiological conditions play a crucial role in the structure and functions of cellular membranes introducing an asymmetry between the inner and outer side of the membrane, which can constitute up to 20% of the total lipids, and second, because DMPA[−] is a lipid widely used in the study of lipid monolayers.^{20,21,9,11,13,22} In this setting, considering that electrostatic interactions control the lipid–lipid interactions in charged lipids,¹⁶ it is expected that different lipid packing associated to their barometric phase transitions can modify noticeably the lipid/water interface.

Thus, the main goal of this work was, in a first instance, to validate the force field of DMPA[−], because as far as we know, this is the first time that this type of lipid has been simulated. To this end, the properties of the bilayer were studied and

* To whom correspondence should be addressed. E-mail: javier.lopez@upct.es.

[†] Universidad de Córdoba.

[‡] Universidad Politécnica de Cartagena, Centro de Electroquímica y Materiales Inteligentes (CEMI).

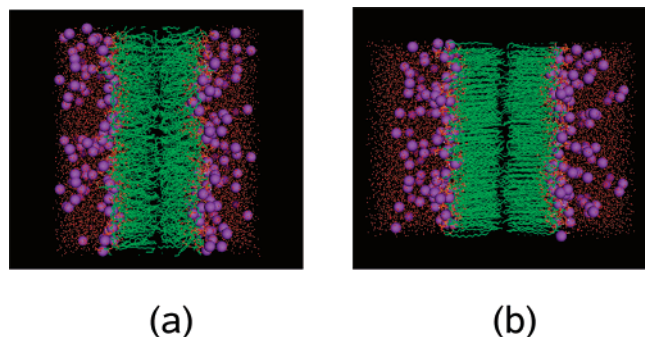


Figure 1. Snapshots of the DMPA⁻ bilayer at two different surface pressures: (a) 0.17mN/m and (b) 40mN/m.

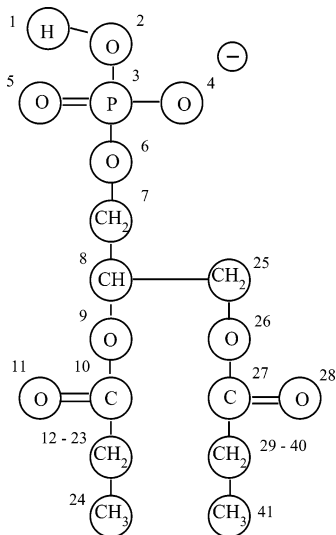


Figure 2. Atom numeration used in this work for a molecule of dimyristoylphosphatidic acid, DMPA^- .

compared with available experimental data. After checking and validating the force field for their liquid crystalline state (L_α), the system was subjected to high-surface pressures, bringing the bilayer close to liquid condensed state (LC), with the goal of describing its barometric behavior. Thus, changes in the lipid structure associated with pressure are described and how these variations affect the lipid/solvent interface properties is discussed.

Assuming that lipid bilayers and monolayers are in fact different physical systems, our hypothesis is that these systems behave differently, and we propose an explanation in terms of lipid–lipid interactions. What we present here is a systematic and detailed study that supports our hypothesis. The obtained results suggest that the simulated system behaves like a bilayer in its liquid crystalline state at low surface pressure but behaves more like a monolayer in its liquid condensed state when subjected to high pressure.

For low surface pressures, the most important lipid interaction is related with lipid tail interdigitation (back-to-back interactions). However, because this kind of interaction is impossible to achieve in a lipid monolayer, monolayers do not reproduce bilayer behavior. However, at higher values of surface pressure, the interdigitation associated with lipid tails vanishes, and the most important effects are related with lateral interaction between neighboring lipids. Thus, at sufficiently high pressures, lipid bilayers and monolayers show the same behavior. In this way, as has been seen for DPPC bilayers,¹⁹ lipid bilayers at high surface pressures reproduce air-water monolayer behavior.

TABLE 1: Charge Density for Each Atom of Lipid DMPA⁻ Molecule, Na⁺ Ions, and SPCE Water Molecules, As Obtained by CNDO Method

molecule	atom number	atom type	charge (<i>e</i>)
DMPA [−]	1	H	0.054
	2	O	−0.460
	3	P	0.680
	4	O	−0.394
	5	O	−0.394
	6	O	−0.434
	7	CH ₂	−0.050
	8	CH	−0.036
	9	O	−0.196
	10	C	0.432
	11	O	−0.164
	12	CH ₂	−0.036
	13–23	CH ₂	0.000
	24	CH ₃	0.000
	25	CH ₂	0.124
	26	O	−0.202
	27	C	0.384
28	O	−0.292	
29	CH ₂	−0.014	
30–40	CH ₂	0.000	
41	CH ₃	0.000	
Ion		Na ⁺	1.000
SPCE water		HW	−0.8476
		OW	0.4238

Finally, a detailed study of the lipid/water interface was carried out for different lipid packing of the membrane.

2. Method and Model

Periodical boundary conditions were considered along the three-dimensional space, X , Y , and Z . The computer simulation box was generated by placing two leaflets of 144 DMPA⁻ (i.e., 288 lipids in total), pointing the lipid heads toward the two water layers placed on both sides of the computing box. Figure 1 depicts two snapshots of the system at two different surface pressures. To maintain the electroneutrality of the system, 288 water molecules were substituted by 288 sodium ions (Na⁺), so that the whole system was constituted by 288 DMPA⁻, 288 Na⁺, and 9780 SPCE water molecules,²³ which amounted 41436 atoms in total.

Gromacs 3.3. package^{24,25} was used to run the MD simulations, and the generated trajectories were analyzed with a software code developed by ourselves. A dipalmitoylphosphatidylserine (DPPS⁻) modified force field¹⁶ was used to carry out these simulations. The charge distribution of a lipid DMPA⁻ molecule was determined by CNDO semiempirical method implemented in HyperChem.²⁶ Thus the charge borne by each atom of the system is depicted in Table 1, corresponding to the atomic numeration shown in Figure 2. Long range interactions were modeled by the Lennard-Jones potential with a cutoff of 0.8 nm, and the electrostatic interactions by the Ewald algorithm.^{27,28} All the bonds of the system were constrained by SHAKE.²⁹ The time step used in all the simulations was 2 fs.

Simulations were carried out on a HPC160 parallel computer using 16 processors with a performance of 1.5 ns of trajectory length per hour.

In this regard, after setting up the system, the whole system was subjected to a steepest descent energy minimization process to remove undesired overlaps between neighboring atoms.

Once the system reached a certain energy minimum, four simulations were carried out at the same normal pressure of 1 atm (z -axis) and each one to different surface pressures (in the X - Y plane of the membrane) at 1, 6, 60, and 225 atm (which correspond to 0.17, 1, 10, and 40 mN/m, respectively). Because

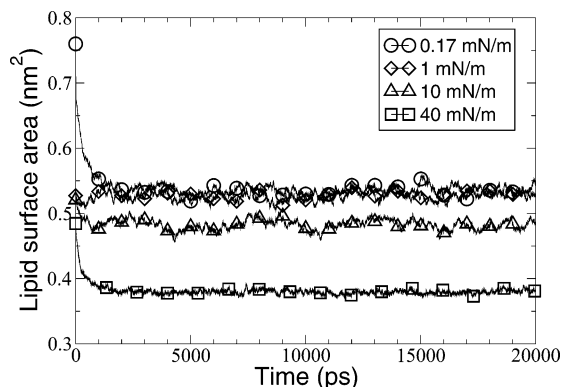


Figure 3. Lipid running area as a function of time for different surface pressures.

a thermodynamic normal temperature and pressure (NTP) state has been simulated, the system was coupled to an external temperature and pressure bath with temperature coupling constants, τ_T , of 0.1 ps and a pressure coupling constant, τ_P , of 1 ps. In both cases, the Berendsen's algorithm was used.³⁰

To avoid undesired simulation artifacts associated to the starting conformation of the system, the first simulation at 0.17 mN/m was carried out at 500 K during 500 ps. The end conformation of this simulation was the starting point at 0.17 mN/m. Next, the system was cooled down to 350 K, and the above-mentioned four simulations were carried out for 20 ns where the end conformation of each trajectory was the starting point of the next simulation at higher surface pressures. In the four cases, the temperature of 350 K is above the DMPA[−] phase transition temperature T_m of 328 K in a range of pH from 4 to 9.³¹ The first 2 ns of trajectory length were discarded for analysis purposes because this was the time required to reach the equilibrium in the four cases.

3. Results and Discussion

3.1. Lipid Area. Figure 3 depicts the area evolution of lipids as a function of time for several surface pressures. From these curves, we observe how for a trajectory length above 2 ns that the system reaches a steady state in the four cases. Thus, the dimension of the equilibrated computing boxes were: (8.82, 8.68, 7.92), (8.76, 8.72, 8.04), (8.38, 8.26, 8.75), and (7.61, 7.41, 10.27), for the x -, y -, and z -axis of the computing box in nm at 0.17, 1, 10, and 40 mN/m surface pressure, respectively.

The area per DMPA[−] molecule obtained from our simulation was compared with experimental data. Note that at low surface pressure, 0.17 mN/m (or 1 atm), the simulated area was 0.54 ± 0.07 nm², which agrees well with the experimental data obtained by Ziegler et al.,³² of 0.58 nm² for its liquid crystalline state L_α . At the same surface pressure, for DMPA[−] air–water monolayers, a surface area of 0.8 nm² was measured from the isotherm surface pressure–lipid area (π –A isotherm) by Lozano et al.³³ When surface pressure is increased to 40 mN/m, the surface area per DMPA[−] molecule obtained by our simulations was 0.40 ± 0.07 nm², which agrees perfectly with the area of 0.4 nm² obtained for monolayer π –A isotherm in its LC state.³³ These results are depicted in Figure 4.

The effect of the interdigitation between opposite lipid leaflets can be observed from the density of methylene groups of lipid tails of the two lipid leaflets, as shown in Figure 5. Thus, we observe how an increase in the surface pressure diminishes the methylene overlap of opposite leaflets, that is, a diminishing in the lipid–lipid interdigitation.

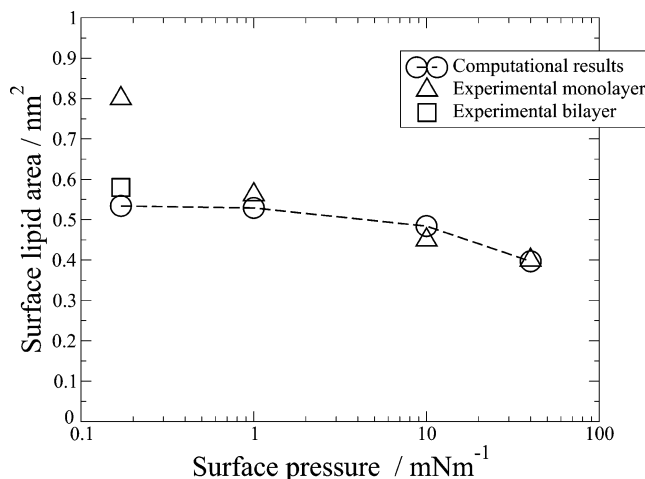


Figure 4. DMPA[−] surface area for different surface pressures: circles represent the simulated data, squares represent the experimental data for a DMPA[−] bilayers, and triangles represent the experimental data for DMPA[−] monolayers.

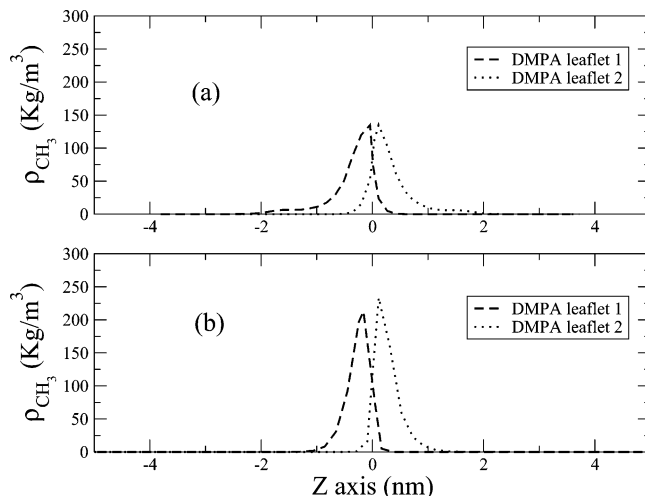


Figure 5. Lipid tail methylene density ρ in kg/m³ along the z -axis for surface pressures of 0.17 mN/m (a) and 40 mN/m (b). The origin of the z -axis was placed in the center of the box.

3.2. Lipid–Lipid Lateral Interactions and Lipid Hydration. The radial distribution function $g(r)$ provides valuable atomic information concerning neighboring molecules. Thus, the radial distribution function $g(r)$ is defined as

$$g(r) = \frac{N(r)}{4\pi r^2 \rho \delta r} \quad (1)$$

where $N(r)$ is the number of atoms in a spherical shell at distance r and thickness δr from a reference atom, and ρ is the number density in the computing box.

Hence, the radial distribution function of the atom numbers 4, 11, and 28 (two carbonyl and a phosphate oxygens) around the phosphorus of a neighboring lipid DMPA[−] was calculated. By integrating the first maximum of the radial distribution function $g(r)$, the coordination numbers of the above-mentioned atoms (4, 11, and 28) over a phosphorus atom as a function of the surfaces pressures were calculated and are depicted in Table 2.

Note that an increase in the surface pressure applied produces an increase in the coordination numbers $N(r)$ between lipids, which clearly reflects the importance of lateral interactions at high values of surface pressures. Indeed, the coordination

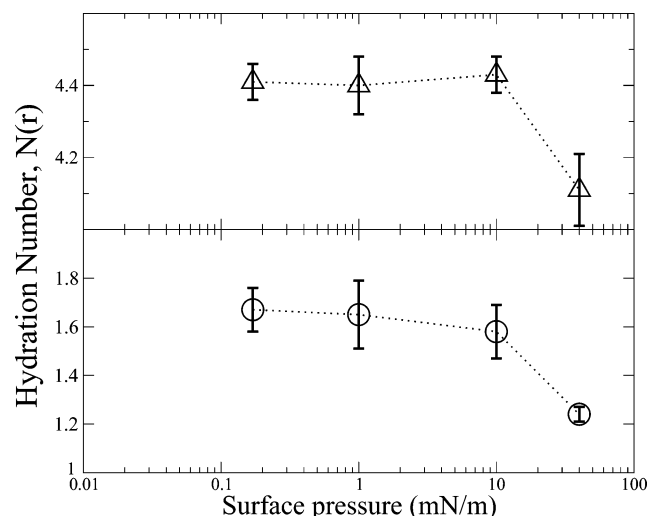


Figure 6. Coordination number for water molecules. Circles, carbonyl oxygens (atom 28), and triangles, phosphate oxygen (atom 4), attending atom numeration of Figure 2.

TABLE 2: Different Values of Coordination Number around the Phosphorus Atoms (Atom 3) by Oxygen Atoms (Atoms 4, 11, and 28) from Neighboring Lipids at Different Value of Surface Pressure

atom number	surface pressure (mN/m)	coordination number
4	0.17	0.26
	1	0.27
	10	0.32
	40	0.45
11	0.17	0.23
	1	0.22
	10	0.25
	40	0.28
28	0.17	0.22
	1	0.23
	10	0.25
	40	0.27

number for atom 4 (phosphate oxygen) around a phosphorus atom undergoes a dramatic increase of 73% from 0.17 to 40 mN/m. Less pronounced is the increase in coordination of the carbonyl oxygens around the phosphorus atom, which is only around 25% under analogous conditions.

The coordination numbers of water oxygens around atoms 4 and 28 of the lipid molecule (oxygen of phosphate and carbonyl group, respectively) are depicted with their standard error in Figure 6. From this figure, we observe that there is no significant variation in the coordination number for pressures ranging from 0.1 to 10 mN/m. For higher pressures (40 mN/m or higher), a dehydration of the polar lipid heads becomes clear. To quantify this effect, the hydration number of the lipid head was calculated from the radial distribution function of water around the heads of the lipid molecules. It was found that 4.20, 4.19, 4.16, and 4.05 water molecules formed the first hydration shell around phosphate oxygen for 0.17, 1, 10, and 40 mN/m, respectively. In regard to the carbonyl oxygen tail, values of 1.12 (for 0.17 mN/m), 1.11 (for 1 mN/m), 1.09 (for 10 mN/m), and 0.85 (for 40 mN/m) were calculated. With these data, lipid hydration (estimated as the sum of the hydration number of the phosphate group) was calculated, reaching a value of 6.44 (for 0.1 mN/m), 6.41 (for 0.17 mN/m), 6.34 (for 10 mN/m), and 5.75 (for 40 mN/m) water molecules. These values agree well with experimental data provided by Schalke et al.⁹ for DMPA[−] air–water monolayers, where the number of water molecules that

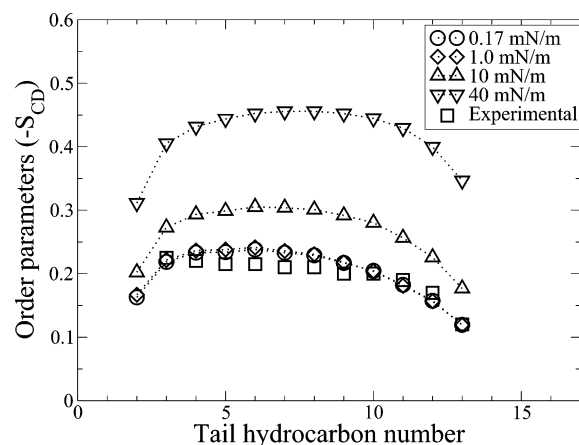


Figure 7. Order parameters ($-S_{CD}$) along hydrocarbon tails for 0.17, 1, 10, and 40 mN/m. The experimental results²⁰ are represented by triangles.

coordinates the lipid head ranges from 6.2 to 4.8 for a surface pressure ranging from 2 to 45 mN/m, respectively.

3.3. Hydrocarbon Tail Structure. The structure of the hydrocarbon tail can be studied in NMR experiments by measuring the deuterium order parameters along the lipid ethylene tails. The order parameter tensor is defined as

$$S_{ab} = \frac{\langle 3 \cos(\theta_a) \cos(\theta_b) - \delta_{ab} \rangle}{2} \quad a, b = x, y, z \quad (2)$$

where x , y , and z are the local coordinates of the system, θ_a is the angle made by the molecular axis with the bilayer normal, and δ_{ab} is the Kronecker delta. From simulation, the order parameter $-S_{CD}$ can be determined using the relation proposed by Egberts and Berendsen³⁴

$$-S_{CD} = \frac{2S_{xx}}{3} + \frac{S_{yy}}{3} \quad (3)$$

where S_{xx} and S_{yy} are the terms of the order parameter tensor of eq 2.

Using eq 3, we can calculate the order parameters of a DMPA[−] molecule for different surface pressures. These results in Figure 7 can be compared with experimental data of the DMPA[−] bilayer in its liquid crystalline state.²⁰ From a comparison simulation with experimental data, we observe the good agreement between both results at low pressures. Moreover, from the simulation we observe how the hydrocarbon structure of the lipid tails is not perturbed at surface pressures up to 1 mN/m. Above this, increasing the surface pressures increases the order of the lipid tails. This increase is more noticeable for pressures above 40 mN/m, corresponding to the pressure at which the barometric transition state of the lipids takes place from its liquid crystalline state (L_α) to gel state (L'_β), which is comparable with the liquid condensed state (LC) in lipid monolayers.

Furthermore, an angle θ was defined as the angle between the vector along the lipid chains and the perpendicular direction to the lipid/water interface. The values of the angle θ obtained were of $\theta = 29.5, 29.7, 22.1$, and 9.2° for 0.17, 1, 10, and 40 mN/m, respectively. In this regard, Schale et al.,⁹ measured an angle θ of 9° at 40 mN/m by X-ray, which agrees well with our simulation results, for pressures at which bilayer and monolayer behaviors converge. In this sense, these data confirm the increasingly packed arrangement found in both monolayer

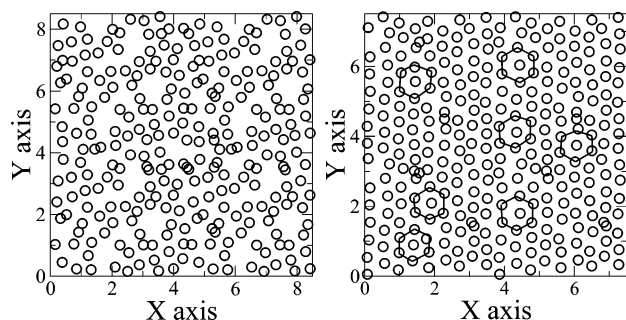


Figure 8. Lipid packing for one of the two DMPA[−] leaflets. Center of mass of each lipid tail is represented by a circle. Left: surface pressure of 0.17 mN/m. Right: surface pressure of 40 mN/m. Lines mark the hexagonal packing of this arrangement.

and bilayer as pressure increases and agrees well with the surface area per lipid reported above.

Considering the lipid packaging, DMPA[−] monolayers are arranged in hexagonal structure at high surface pressures. In Figure 8, the center of mass of the ethylene lipid tails is plotted in the *X*–*Y* plane (lipid plane). The hexagonal structure associated with the gel structure L'_β (in bilayers) and liquid condensed state LC (in monolayers) can be clearly seen for a pressure of 40 mN/m.

In addition, the lipid head orientation with respect to the normal to the lipid plane was studied, obtaining values of 49.7, 48.8, 42.3, and 44.7° at 0.17, 1, 10, and 40 mN/m respectively. These values show how the DMPA[−] heads in their liquid crystalline state are much more oriented toward the water layer than DPPC, where an orientation almost parallel to the surface of the lipid layer has been reported.^{10,19} This increase in head orientation can be explained by the greater degree of head hydration and lipid packaging of them than the DPPC ones. In this regard, Schalke et al.⁹ reported that the head orientation of DMPA[−] in its liquid condensed state LC for a pressure of 40 mN/m was 47°, which agrees with our simulation result of 44.7°. Unfortunately, no experimental data of DMPA[−] head orientation in bilayers has been reported to compare with its liquid crystalline state L_α .

By means of FTIR, Lozano et al.³³ observed that in the monolayers of pure DMPA[−] at high surface pressures the transition dipole moment of the carbonyl group aligned with the interface. The angular distribution function of the bonding vector for this C=O group was calculated for each surface pressure studied. Thus, from Figure 9 we can observe that for high pressures, for example, 40 mN/m, the distribution takes a sharper form with two maximum peaks at 90 and 97°, reflecting the above-mentioned change in orientation of the carbonyl moiety. This dense packing of a DMPA[−] monolayer at high surface pressure is in a perfect accordance with experimental data.

3.4. Electrostatic Potential. The electrostatic potential ψ across the lipids layers was computed from the double integral of the charge density³⁵

$$\psi(z) - \psi(0) = -\frac{1}{\epsilon_0} \int_0^z dz' \int_0^{z'} \rho(z'') dz'' \quad (4)$$

where the origin *z* of the electrostatic potential $\psi(0)$ is taken at the middle of the lipid bilayer. The electrostatic potential computed in this way agrees with the computed charge density using Poisson's equation without using a cutoff radius.³⁶ Hence, Figure 10 depicts the electrostatic potential averaged on both symmetric lipid leaflets.

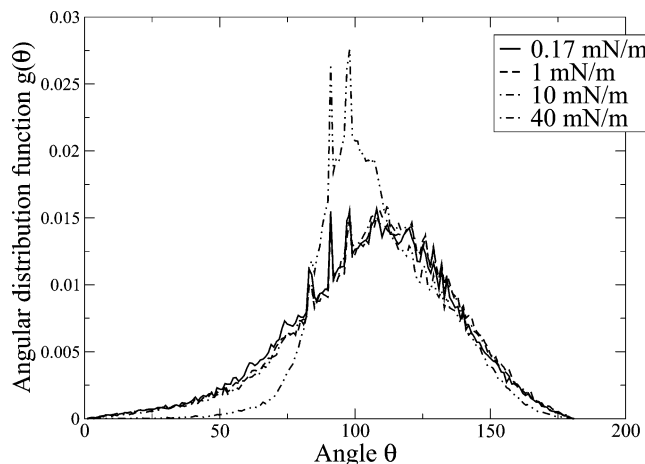


Figure 9. Angular distribution function for the vector bonding of the C=O moiety (atoms 27 and 28, considering the atom numeration of Figure 2) with respect to the perpendicular axis to the lipid/water interface and different surface pressures.

Of note is the dramatic effect of surface pressure on the potential difference at the interface, which ranges from −0.08 V at 0.17 mN/m to −0.22 V at 40 mN/m, an effect that is of great relevance in the electrochemistry for developing modified electrodes using Langmuir–Blodgett's method.³⁷

3.5. Solution Properties. Having established the lipid structure associated to barometric transitions, the way in which the solution properties are perturbed by the barometric isomorphic lipid transition was studied. For that purpose, the computation box was sliced to 19 slabs parallel to the *X*–*Y* plane (lipid leaflet), so that slab number 10 matched the middle of lipid bilayer.

3.5.1. Water and Sodium (Na⁺) Translational Diffusion Coefficient, D_t . First, the diffusion coefficients of water and Na⁺ ions were calculated using the treatment described by Cascales et al.,¹⁶ which permitted us to estimate their diffusion coefficient in each zone of the computing box. The results for water are shown in Figure 11. As we can see, the regions on both sides of the box are composed of bulk water, reaching a steady value for the $D_{t,xy}$. Note that the diffusion coefficient of bulk water for SPC at 349 K is $7.5 \times 10^{-5} \text{ cm}^2 \text{ s}^{-1}$,³⁸ which is very close to our value of $6.5 \times 10^{-5} \text{ cm}^2 \text{ s}^{-1}$. Also of interest is that there is no significative variation in the water diffusion coefficient with respect to pressure, indicating that our conclusions are not affected by any simulation artifact. From the results depicted in Figure 11, it can be observed that there is almost no correlation between the diffusion coefficient and surface pressure at the lipid/water interface, where a minimum value of around $2.5 \times 10^{-5} \text{ cm}^2 \text{ s}^{-1}$ was measured in the four cases in the vicinity of the lipid interface regardless of the isomorphic state of the lipids.

A similar trend was observed for Na⁺ ions, where the values of 4.5, 4.3, 4.2, and $4.4 \times 10^{-5} \text{ cm}^2 \text{ s}^{-1}$ were measured for the bulk water and 1.2, 1.1, 1.2, and $1.2 \times 10^{-5} \text{ cm}^2 \text{ s}^{-1}$ in the vicinity of the lipid surface, respectively. These results are in good agreement with experimental data for sodium ion in bulk water³⁹ and in the vicinity DPPS[−] layers,⁴⁰ where values of $3.8 \times 10^{-5} \text{ cm}^2 \text{ s}^{-1}$ have been reported for bulk water at 298 K and a value of $2.1 \pm 1.1 \times 10^{-5} \text{ cm}^2 \text{ s}^{-1}$ in the vicinity of a DPPS[−] bilayer at 350 K.

The first conclusion from the values reported above is that the barometric phase transition of lipids does not perturb the profile of sodium diffusion from the bulk water to the vicinity of the lipid interface.

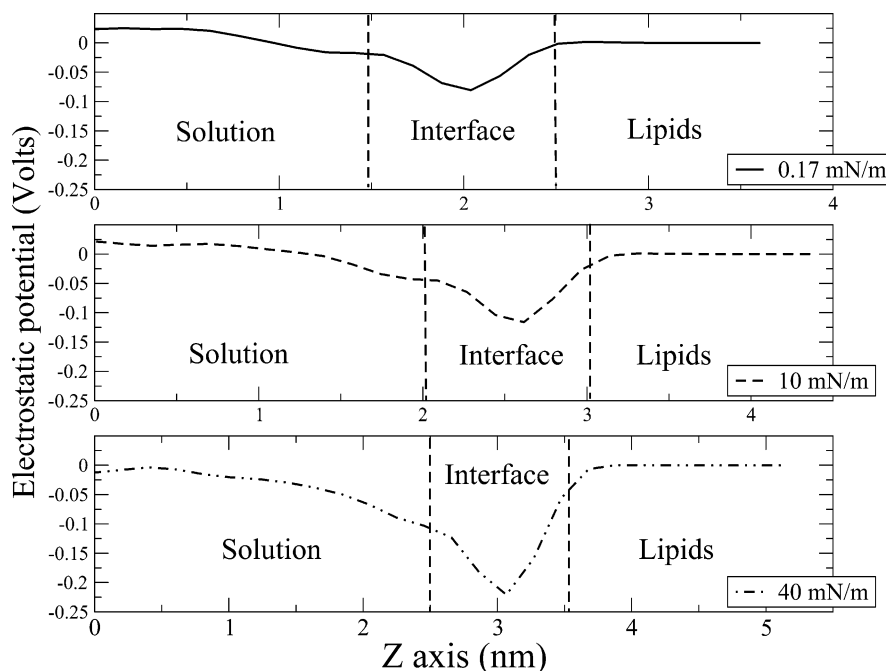


Figure 10. Electrostatic potential across the z -axis for each surface pressure. For clarity, each region is delineated with dotted lines. The zero volts is placed in the middle of the water layer.

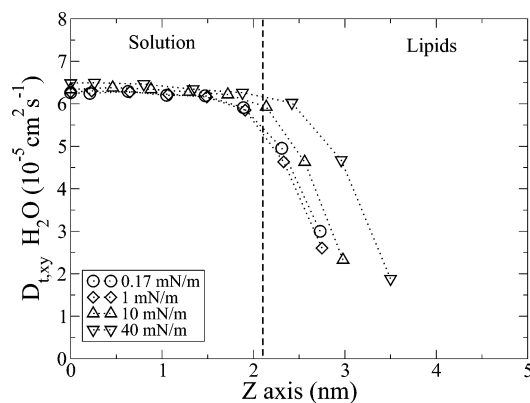


Figure 11. Translational diffusion coefficient $D_{\text{H}_2\text{O}}$ of water for different positions in the computing box along the axis perpendicular to the lipid/water interface and different surface pressures.

3.5.2. *Water Rotational Relaxation Time, τ .* Using the same regions as described above, we estimated the rotational diffusion coefficient of water molecules.¹⁶ The reorientation of water molecules is described by the correlation function

$$\langle P_1(t) \rangle = \sum_{i=1}^3 a_i \exp(-t/\tau_i) \quad (5)$$

from which an apparent mean relaxation time, τ_{app} , can be obtained

$$\tau_{\text{app}} = \frac{\sum_{i=1}^3 a_i \tau_i}{\sum_{i=1}^3 a_i} \quad (6)$$

Within this procedure, we calculated τ_{app} from the beginning of the lipid/water interface to bulk water at each surface pressure (see Table 3). As an example, the fit of the calculated data to

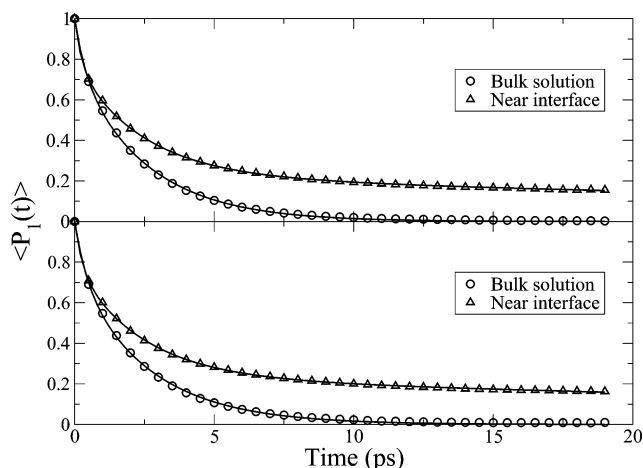


Figure 12. Reorientational correlation function of water dipole at 0.17 mN/m (top) and 40 mN/m (down) surface pressures. Symbols: simulation results. Line: fitted curve.

TABLE 3: Reorientational Relaxation Time (τ_{app}) of Water for Different Regions of the Computing Box and Surface Pressures

slab number	$\tau_{\text{app}}/\text{ps}$ π (mN/m)			
	0.17	1	10	40
4	11.85	9.82	10.98	12.64
5	7.77	9.21	7.75	6.79
6	3.81	4.73	5.06	3.56
7	2.32	2.56	2.28	2.07
8	2.09	2.30	2.12	2.07
9	2.04	2.05	2.04	2.03
10	2.11	2.09	2.07	2.04

eq 6 for 0.17 and 40 mN/m in the central region and near the lipid/water interface is depicted in Figure 12.

The assumption of bulk water in the middle of the aqueous region and the absence of any simulation artifact due to surface pressure is again confirmed by this study. The 2.11 ps of our simulated value is in good agreement with the 1.7 ps³⁸ reported for bulk water at 349 K. The slight difference between the results

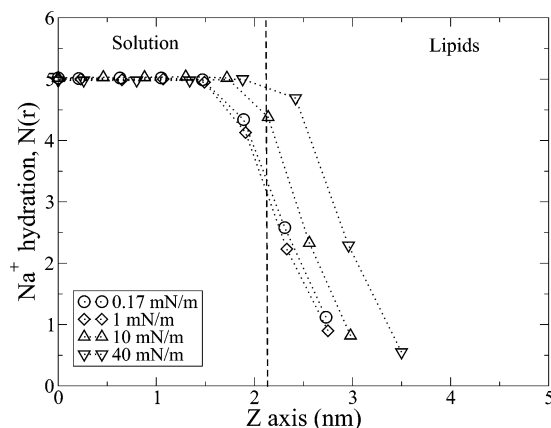


Figure 13. Values of coordination number for water molecules surrounding the Na^+ ions for different surface pressures and regions of the computing box.

can be attributed to the fact that in our simulations some water molecules that were hydrating sodium ions were considered rather than the pure water in Postma's work.³⁸ In regard to the rotational relaxation time in the vicinity of the lipid surface, it increased up to 11.3 ± 1.1 ps independently of the surface pressure. In other words, we can assert that lipid barometric phase transition did not perturb the dynamic properties of water from bulk to water/lipid interface in the range of pressures studied.

3.5.3. Sodium Ion Hydration. Using the radial distribution function of eq 1, we are able to calculate the hydration number of sodium ions in solution. As it is shown in Figure 13, a value of 5.0 water molecules was estimated in bulk water and 1.0 water molecule near the lipid/water interface. The results for bulk water agree well with experimental⁴¹ and simulation⁴² data in aqueous solution, where values of 4.6 and 3.8 have been reported at 298 K. At the lipid/water interface, Cascales et al. reported⁴⁰ a value of 1.2 in the vicinity of a DPPS⁻ bilayer, which agrees with the value of 1.1 obtained here for all the simulated surface pressures.

4. Conclusions

Four DMPA⁻ bilayers were subjected to different lateral pressures in a range from 0.17 to 40 mN/m. The results demonstrated that the lipid bilayer and monolayer follow the same behavior only when surface pressure is sufficiently high. On the other hand, their behavior differed with low pressures.

Validation of the DMPA⁻ force field was made by comparison with experimental data for both bilayer and monolayer. The experimental data corresponding to hydrocarbon order parameters and surface area per lipid molecule showed excellent agreement with our simulation results at low surface pressures, which reproduced the DMPA⁻ bilayer behavior. At high surface pressures, the area per lipid molecule, orientation of the carbonyl moiety, tail orientation, head orientation, and hexagonal arrangement of the lipid tails reflected monolayer behavior in the liquid condensed (LC) phase.

In addition, we focused our interest on how this barometric polymorphic phase transition affects the lipid/solution interface. Thus, the water reorientational time, the water and sodium translational diffusion coefficient, and sodium hydration were studied. From the simulation results, we can assert that barometric polymorphic lipid transition does not perturb the lipid/water interface properties in the range of the pressures studied.

Acknowledgment. J.J.L.C. wishes to thank the Spanish Government (Ministerio de Educacion y Ciencia, MEC) and Fundacion Seneca for his financial support through projects BQU-2001-04777 and 00483/PI/04, respectively. L.C., M.T.M.R., and J.J.G.C. thank the Spanish CICYT for financial support of this research in the framework of Project Nos. CTQ2004-03246/BQU and MAT2004-03849. Also, J.J.G.C. thanks the Ministerio de Educacion y Ciencia for a Formacion Profesorado Universitario (FPU) predoctoral fellowship.

References and Notes

- (1) Cullis, P.; Hope, M.; de Kruijff, B.; Verkleij, A.; Tilcock, C. In *Phospholipids and cellular regulation*; Kuo, J., Ed.; CRC Press: Boca Raton, FL, 1985; pp 1–60.
- (2) Yeagle, P. *FASEB J.* **1989**, *3* (4), 1833–1842.
- (3) Nagle, J.; Tristram-Nagle, S. *Biochim. Biophys. Acta* **2000**, *1469* (3), 159–195.
- (4) Yeagle, P. L. In *The structure of biological membranes*; Yeagle, P., Ed.; CRC Press: Boca Raton, FL, 1992; pp 73–156.
- (5) Ichimori, H.; Hata, T.; Matsuki, H.; Kaneshina, S. *Biochim. Biophys. Acta* **1998**, *1414* (1–2), 165–174.
- (6) R. Winter. *Curr. Opin. Colloid Interface Sci.* **2001**, *6* (3), 303–312.
- (7) Möhwald, H. In *Handbook of biological physics*; Lipowsky, R., Sackmann, E., Eds.; Elsevier Science B. V.: New York, 1995; pp 161–211.
- (8) Hunt, R.; Mitchell, M.; Dluhy, R. *J. Mol. Struct.* **1989**, (214), 93–109.
- (9) Schalke, M.; Krüger, P.; Weygand, M.; Lösche, M. *Biochim. Biophys. Acta* **2000**, *1464*, 113–126.
- (10) Dluhy, R. *Appl. Spectrosc. Rev.* **2000**, *35* (4), 315–351.
- (11) Schalke, M.; Lösche, M. *Adv. Colloid Interface Sci.* **2000**, *88* (1–2), 243–274.
- (12) Mendelsohn, R.; Flach, C. *Curr. Top. Membr.* **2002**, (52), 57–88.
- (13) Pedrosa, J.; Perez, M.; Prieto, I.; Martin-Romero, M.; Möbius, D.; Camacho, L. *Phys. Chem. Chem. Phys.* **2002**, *4* (11), 2329–2336.
- (14) van Gunsteren, W. F.; Berendsen, H. J. C. *Angew. Chem., Int. Ed. Engl.* **1990**, *29* (9), 992–1023.
- (15) Alper, H. E.; Bassolino-Klimas, D.; Stouch, T. R. *J. Chem. Phys.* **1993**, *99* (7), 5554–5559.
- (16) Cascales, J.; Berendsen, H.; Garcia de la Torre, J. *J. Phys. Chem.* **1996**, *100* (21), 8621–8627.
- (17) Tieleman, D.; Marrink, S.; Berendsen, H. *Biochim. Biophys. Acta* **1997**, *1331* (3), 235–270.
- (18) Kaznessis, Y.; Kim, S.; Larson, R. *Biophys. J.* **2002**, *82* (4), 1731–1742.
- (19) Cascales, J. L.; Otero, T.; Romero, A. F.; Camacho, L. *Langmuir* **2006**, *22* (13), 5818–5824.
- (20) Pott, T.; Maillet, J.; Dufourc, E. *Biophys. J.* **1995**, *69* (5), 1897–1908.
- (21) Wu, F.; Gericke, A.; Flach, C.; Mealy, T.; Seaton, B.; Mendelsohn, R. *Biophys. J.* **1998**, *74*, 3273–3281.
- (22) Mendelsohn, R.; Flach, C. *Curr. Top. Membr.* **2002**, *52*, 57–78.
- (23) Berendsen, H.; Grigera, J.; Straatsma, T. *J. Phys. Chem.* **1987**, *91* (24), 6269–6271.
- (24) Lindahl, E.; Hess, B.; van der Spoel, D. *J. Mol. Model.* **2001**, *7* (8), 306–317.
- (25) Berendsen, H.; van der Spoel, D.; van Drunen, R. *Comp. Phys. Comm.* **1995**, *91* (1–3), 43–56.
- (26) Hyperchem 7.5. HyperCube, Inc.
- (27) Darden, T.; York, D.; Pedersen, L. *J. Chem. Phys.* **1993**, *98* (12), 10089–10092.
- (28) Essmann, U.; Perea, L.; Berkowitz, M.; Darden, T.; Lee, H.; Pedersen, L. *J. Chem. Phys.* **1995**, *103* (19), 8577–8593.
- (29) van Gunsteren, W.; Berendsen, H. *Mol. Phys.* **1977**, *34* (5), 1311–1327.
- (30) Berendsen, H. J. C.; Postma, J. P. M.; van Gunsteren, W. F.; DiNola, A.; Haak, J. R. *J. Chem. Phys.* **1984**, *8* (8), 3684–3690.
- (31) Blume, A.; Eibl, H. *Biochim. Biophys. Acta* **1979**, *558*(1), 476–488.
- (32) Ziegler, W.; Blume, A. *Spectrochim. Acta, Part A* **1995**, *51*, 1763–1778.
- (33) Lozano, P.; Fernandez, A.; Ruiz, J.; Camacho, L.; Martin, M.; Muñoz, E. *J. Phys. Chem. B* **2002**, *106* (25), 6507–6514.

- (34) Egberts, E.; Berendsen, H. *J. Chem. Phys.* **1988**, *89* (6), 3718–3732.
- (35) van Buuren, A.; Berendsen, H. *Langmuir* **1994**, *10* (6), 1703–1713.
- (36) Pandit, S.; Bostick, D.; Berkowitz, M. *Biophys. J.* **2003**, *84* (6), 3743–3750.
- (37) Goldenberg, L. *J. Electroanal. Chem.* **1994**, *379* (1–2), 3–19.
- (38) Postma, J. A molecular dynamics study of water. Ph.D. Thesis, Rijkuniversiteit Groningen, The Netherlands, 1985.
- (39) Lide, D., Ed. *Handbook of Chemistry and Physics*; CRC Press: Boca Raton, FL, 2002.
- (40) Cascales, J. L.; de la Torre, J. G. *Biochim. Biophys. Acta* **1997**, *1330* (2), 145–156.
- (41) Bockris, J.; Reddy, A. *Modern Electrochemistry I. Ionics*; Plenum Press: New York, 1998.
- (42) Impey, R.; Madden, P.; McDonald, I. *J. Phys. Chem.* **1983**, *87* (25), 5071–5083.